A Letters Journal Exploring the Frontiers of Physics

March 2020

EPL, **129** (2020) 58004
doi: 10.1209/0295-5075/129/58004

www.epljournal.org

All-passive nonlinear electromagnetic metastructure for simultaneous energy harvesting and earthquake mitigation

Jingfan Chen and Ya Wang[a]

J. Mike Walker' 66 Department of Mechanical Engineering, Texas A&M University - 202 Spencer St, College Station, TX, 77843, USA

received 20 November 2019; accepted in final form 27 March 2020
published online 6 April 2020

PACS 85.80.Jm – Magnetoelectric devices
PACS 88.90.+t – Other topics in renewable energy and applications
PACS 07.10.Fq – Vibration isolation

Abstract – Resonance-based metastructures have recently attracted increasing attention for earthquake mitigation. Their application is limited, however, by their narrow attenuation zone. In this letter, we report an all-passive metastructure consisting of an array of dual-functional nonlinear electromagnetic resonator units. Each resonator unit consists of two rotary oscillators and one rectilinear oscillator based on nonlinear magnet levitation. The nonlinearity and intrinsic frequency up-conversion allows a broadened frequency operation range for simultaneous earthquake mitigation and energy harvesting. An analytical model is developed to investigate the wave dispersion and dynamic response of a single nonlinear resonant unit and the results agree well with the experimental data and the finite element analysis (FEA). Experimental results show that a two-unit array maintains a high instantaneous output voltage from 2.5 to 4.5 Hz under base excitation of 0.5 g. Maximum power of 3.7 mW and harvesting efficiency of 22.26% are achieved under harmonic excitation of 0.5 g and 4 Hz. The FEA exhibits the displacement reduction over 6 dB from 3.5 to 7 Hz with the metastructure array of 1340 units (160 meters long).

Introduction. – Millions of earthquakes occur around the world each year, typically generating vibrational energy at 1–20 Hz. Major earthquakes, greater than magnitude 7, release the energy equivalent to 476 million kilograms of explosive, weakening or even making buildings and other infrastructures collapse that are not resistant to large vibration [1]. Recently, phononic crystals, which are artificially engineered materials with periodic patterns [2], and resonance-based metastructures have proposed as new approach for earthquake mitigation. Some large-scale phononic crystals consisting of periodic arrays of cylindrical holes [3] or cross-like cavities [4] have demonstrated their ability in reflecting seismic elastic energy or rerouting surface waves within certain frequency range. However, their application at low frequencies is limited because that often requires an impractical periodicity length to create desired band gaps. Resonance-based metastructures take advantage of local resonant masses to absorb energy around their resonances, allowing much smaller units to be used to obtain approximately the same band gaps as phononic crystals. Among them, periodic foundations and resonance-based barriers have been greatly investigated to promote their functionality in seismic shielding [5–7]. Periodic foundations based on a chain mass-in-mass configuration integrate directly with the foundation of a building, creating an isolation system that reduces the energy transferred from a seismic wave to the building [8,9]. However, those seismic isolation systems can only be employed with new buildings and only protect the individual specific buildings. Different from periodic foundations, resonance-based barriers, which usually consist of a mass suspended by springs, were realized by burying sub-wavelength local linear resonators under the soil surface [10,11]. The seismic waves propagating in soils were shielded in a frequency band located around the resonant frequency of the linear resonators, and thus the selected surrounding areas were protected from the incoming wave. The band gaps created by linear resonant metastructures, however, were confined to a narrow frequency bandwidth, that is, the energy from multi-frequency seismic wave may not be sufficiently captured. Creating an array of resonators with multiple distributed resonance

[a]E-mail: ya.wang@tamu.edu

frequencies was proposed to enable a wider spectrum [12], but this complicates the structure design and affects the attenuation efficiency. Nonlinear resonators [13,14] and frequency up-conversion strategies [15–17] have been proposed to broaden the bandwidth and improve the efficiency of energy harvesters, however, these methods are rarely applied for earthquake mitigation due to several practical challenges. One of the biggest challenges is how to provide a sustainable and reliable power supply. Though several techniques have been reported to harvest energy from seismic vibrations [18,19], with the hope to provide backup power during an earthquake, there are still unsolved issues such as limited power efficiency and narrow bandwidth. In this letter, we proposed the concept of simultaneously harvesting and mitigating the seismic vibrations in a single device over a wide frequency range.

This model. – In this letter, we report the design of an electromagnetic metastructure with intrinsic frequency up-conversion and nonlinear properties to realize the concept of simultaneous energy harvesting and earthquake mitigation. The all-passive metastructure consisting of an array of nonlinear resonators is designed to be buried under the soil surface (fig. 1(a)). The nonlinear design leads to an attenuation zone in which the wave propagation is passively suppressed. By coupling with the electromagnetic field, the kinetic energy is further converted into electrical energy. Figure 1(b) illustrates the schematic of a two-unit dual-functional resonator array. Each dual-functional resonator unit consists of two rotary oscillators ($\mathrm{R}_T\mathrm{O}_{j,i,1}$ and $\mathrm{R}_T\mathrm{O}_{j,i,2}$), j is equal to 1 or 2 that means the first or second row of the resonator, and i is equal to 1 to N that means the i-th column, coupled through one rectilinear oscillator ($\mathrm{R}_L\mathrm{O}_i$). The $\mathrm{R}_T\mathrm{O}$ consists of a stator and a rotor, where the stator has 8 coils (2000 turns) connected in series, while the rotor is made up of 8 cube permanent magnets centrally symmetric distributed with alternating poles arrayed adjacently. The comparison of a different number of magnets can be found in the Supplementary Material `Supplementarymaterial.pdf` (SM). The $\mathrm{R}_L\mathrm{O}$ includes one moving magnet and two stationary magnets (brakes) stacked by the same pole facing each other to form the magnetic levitation system, which enables its operation over a wider frequency range. Each stationary magnet is shared by two adjacent units, and is excited by the base, as shown in fig. 1(c). As discussed in our previous studies [20,21], the slight movement of the moving magnets can cause a significant change in the driving torque applied on the rotors, thus the rotors is able to rotate at high speed through intrinsic frequency up-conversion and generate a large voltage output. By exploiting the nonlinearity and the intrinsic frequency up-conversion of each unit, an array of such dual-functional resonators can be buried under the soil surface to passively absorb and harvest a broader band frequency of vibrations and turn it into directly usable electricity.

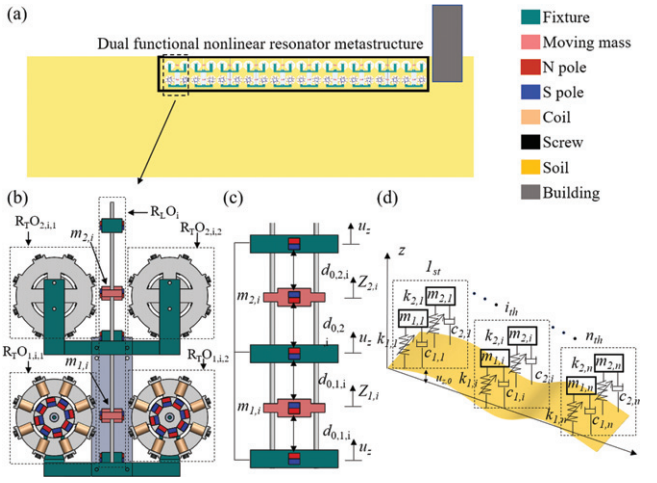

Fig. 1: (a) Schematic of the metastructure buried under the soil surface. (b) Mechanical schematic diagram of dual functional resonator array. (c) Magnets configuration of the $\mathrm{R}_L\mathrm{O}$. (d) The theoretical model of multiple resonators interacting with soil.

The magnetic repulsive force applied to each cuboidal magnet can be obtained analytically according to Akoun's theory [22]. The magnetic repulsive force is curve fit as a function of the surface distance d between two magnets,

$$F = 42.12e^{-142.50d}. \tag{1}$$

The equilibrium position Z_e of the moving magnet and the linearized frequency is related to the mass of the moving magnet and the preset distance d_0 between the two magnets. Thus, the bandwidth of the resonator can be adjusted accordingly. Detailed derivation can be found in the SM.

As shown in fig. 1(d), the soil is modelled as an elastic half-space ($z < 0$) [23] and connected to local resonators, with mass $m_{j,i}$, nonlinear contact stiffness and damping. The equation of motion for the i-th dual-functional resonator unit on row j under base excitation can be written as

$$\begin{aligned} &m_{j,i}\ddot{Z}_{j,i} + c_{j,i}\left(\dot{Z}_{j,i} - \dot{u}_{z,0}\right) = -m_{j,i}g \\ &+42.12e^{-142.50(d_0+Z_e+Z_{j,i}-u_{z,0})} \\ &-42.12e^{-142.50(d_0-Z_e-Z_{j,i}+u_{z,0})}, \end{aligned} \tag{2}$$

where the dot represents a derivative with respect to time, d_0 is the preset distance between two magnets. $Z_{j,i}$ and $u_{z,0}$ are the displacement of the moving magnet and the soil surface, respectively. Z_e is the static equilibrium and $g = 9.81\,\mathrm{m/s^2}$ is the gravitational constant.

Let $y_{j,i} = Z_{j,i} - u_{z,0}$ and substitute into eq. (2) to obtain a governing equation written in terms of the relative displacement between the moving magnet and the soil,

$$\ddot{y}_{j,i} + \frac{c_{j,i}}{m_{j,i}}\dot{y}_{j,i} = f_0 + f_{j,i} + f_1\cos\omega t, \tag{3}$$

Table 1: Design parameters of the nonlinear resonator unit.

Symbol	Description	Value
m	Mass of the moving magnet	250 g
c_1	Damping of the rectilinear oscillation	0.3 kg/s
d_0	The preset distance between two magnets	70 mm
Z_e	The static equilibrium position	−20 mm
f_1	The external acceleration	$0.5g$

where

$$f_0 = -g \tag{4}$$

$$f_{j,i} = \frac{42.12}{m_{j,i}} e^{-142.50(d_0+Z_e+y_{j,i})} - \frac{42.12}{m_{j,i}} e^{-142.50(d_0-Z_e-y_{j,i})}, \tag{5}$$

$$f_1 = \omega^2 u_{z,0}. \tag{6}$$

The nonlinear system of eq. (3) has no known closed form solution. By solving it numerically in Matlab using the parameters shown in table 1, the steady-state displacement of the system yields the results shown in fig. 2(a).

The resonator exerts a vertical force on the soil, at the surface $z = 0$, the boundary conditions are

$$\sigma_{zz,i} = \frac{m_{j,i} f_{j,i}}{A}, \quad \sigma_{xz,i} = 0, \tag{7}$$

where σ_{zz} and σ_{xz} are the stress tensors acting on the surface in the z- and x-direction, respectively, and A is the acting area.

The wave dispersion for the soil with coupled nonlinear resonator is derived following the elastic wave propagation model in a semi-infinite media [24], but a nonlinear stress tensor is used to exhibit its nonlinearity:

$$\left(2 - \frac{\omega^2}{k^2 c_T^2}\right)^2 - 4\left(1 - \frac{\omega^2}{k^2 c_L^2}\right)^{\frac{1}{2}} \left(1 - \frac{\omega^2}{k^2 c_T^2}\right)^{\frac{1}{2}} = \frac{m_{j,i} f_{j,i}}{A\rho u_{z,0}} \frac{\omega^2}{k^3 c_T^4} \left(1 - \frac{\omega^2}{k^2 c_L^2}\right)^{\frac{1}{2}}. \tag{8}$$

Here ρ is the density of the soil, c_L and c_T are the wave propagation speed in the longitudinal and transverse direction, k is the wavenumber propagating along the x-direction, and ω is the wave frequency. The detailed derivation steps can be found in the SM.

Unlike the linear resonator, where the wave is totally blocked around its resonance [25], the nonlinear resonator allows the wave energy to be stored and dissipated over a wider attenuation zone. The energy transferred from the seismic wave to the resonator can be expressed as

$$E_{j,i} = Work = \int m_{j,i} f_1 \mathrm{d}y_{j,i}, \tag{9}$$

which is the positive correlation with the steady state displacement. As shown in fig. 2(a), one demonstrates that the wave energy is stored in the nonlinear resonator over a large attenuation zone.

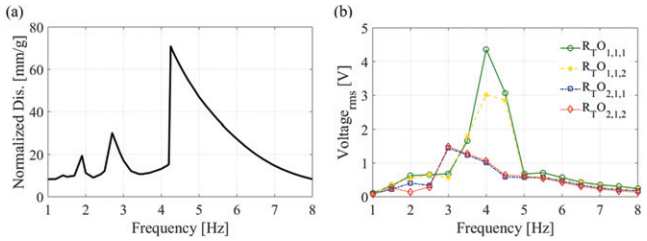

Fig. 2: (a) Numeric simulation result of the normalized steady displacement of the moving magnet under different excitation frequency from 1 to 8 Hz. (b) Experimental voltage RMS output of four R$_T$O's under different excitation frequency from 1 to 8 Hz.

Results. – To provide a deeper insight into the harvesting capacity of the resonator unit, one end of the two-unit array is attached to an electrodynamic long stroke shaker (APS 113, APS Dynamics Inc.). The harmonic base excitation is provided by a wave generator (33500B, Keysight Technologies, Inc.) in conjunction with a power amplifier (APS 125, APS Dynamics Inc.) and measured by an accelerometer (333B32, PCB Piezotronics, Inc.). The output voltage of the two-unit resonator array is recorded by an oscilloscope (DSOX2024A, Keysight Technologies, Inc.). From our previous study [20], at the excitation level of $0.1g$, the input acceleration was insufficient to transfer the linear motion into high frequency rotation, which resulted in low voltage output. For the acceleration level of $0.3g$, $0.5g$, and $0.7g$, the voltage output increased proportionally as the acceleration level increased. Since typical accelerations in earthquakes are between 0.05 and $1g$, and few buildings would survive an acceleration of more than $0.5g$, the excitation amplitude of $0.5g$ was chosen for the experiment. Figure 2(b) shows the root mean square (RMS) voltage of the four R$_T$O's subject to the base excitation of $0.5g$ between 1.0 to 8.0 Hz. Both the R$_T$O$_{1,1,1}$ and R$_T$O$_{1,1,2}$ have a maximum RMS voltage output V_{rms} greater than 3 V at 4 Hz, and the R$_T$O$_{2,1,1}$ and R$_T$O$_{2,1,2}$ have a maximum V_{rms} of 1.5 V at 3 Hz, indicating that a larger voltage output can be achieved by connecting these R$_T$Os after circuit rectification. In addition, the peak output occurs at around 4 Hz, which is close to the linearized frequency of the resonator (6 Hz). The excited frequency of the output peak is slightly different from the numerical simulation result of steady-state displacement, possibly due to the neglect of friction and magnetic force between the rotor and the moving magnet in the analytical model.

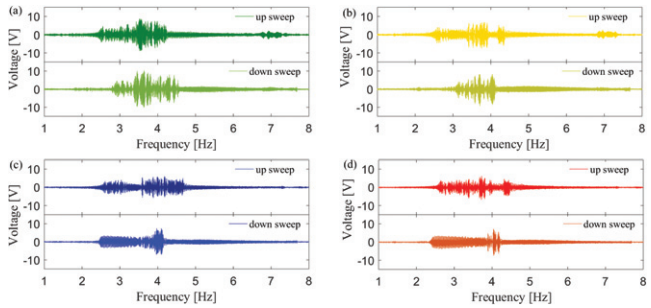

Fig. 3: Experimental results of frequency up and down sweep of (a) $R_TO_{1,1,1}$; (b) $R_TO_{1,1,2}$; (c) $R_TO_{2,1,1}$; (d) $R_TO_{2,1,2}$ under the base acceleration of $0.5g$.

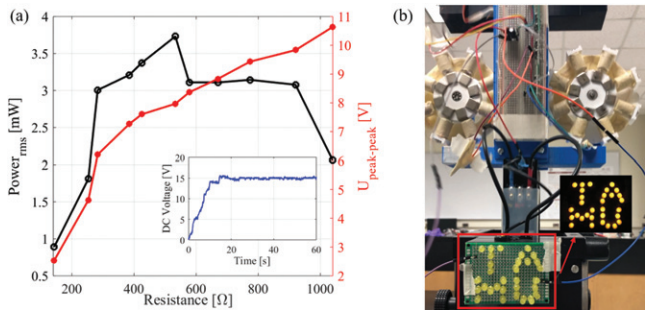

Fig. 4: (a) Power RMS and voltage peak to peak *vs.* load resistance. The insert figure is the DC output voltage after four bridge circuits at 4 Hz and $0.5g$. (b) LEDs were powered with full brightness.

A series of linear frequency sweep experiments are conducted from 1.0 Hz to 8.0 Hz at a 0.05 Hz/s sweep rate. Figure 3 shows the response of the four R_TO's subject to the base excitation level of $0.5g$. A large instantaneous voltage output is found and maintained from 2.5 to 4.5 Hz.

In the power generation test, $R_TO_{1,1,1}$ is first connected to a series of resistive loads. As shown in fig. 4(a), under the harmonic excitation of $0.5g$ and 4.0 Hz, the maximum RMS power output is 3.7 mW at the optimum load resistance of 533 Ω. The power efficiency, η_H, defined as the ratio of electrical power out to mechanical power in [26], returns

$$\eta_H = \frac{4\frac{U_{peak}^2}{R_{optimal}}}{\omega m_{j,i} a_{max} d_0} = 22.26\%, \tag{10}$$

where U_{peak} is the peak-to-peak voltage, $R_{optimal}$ is the optimal load resistance and a_{max} is the maximum input acceleration.

Then, the output of each R_TO is converted to direct voltage (DC) via a rectifier bridge and connected in serial to both ends of a capacitor (100 μF). The DC voltage of the four R_TO's is measured and plotted in fig. 4(a) (inset). After 15 seconds, the voltage maintains about 15 V, which indicates the possibility of manufacturing multiple R_TO's to increase power output and convert the vibration to stable electric power. The array of two dual-functional resonators is used as a direct power supplier for LEDs (Kingso, Forward voltage/current: 2.8–3.6 V/20 mA), which are illuminated as shown in the supplementary movie `tamu_light.mp4` and in fig. 4(b).

A 2D plane strain model is built in COMSOL Multiphysics® to explore the mitigation performance of the proposed metastructure array. The vertical displacements of the surface ground motion are evaluated and compared for the cases buried without and with the metastructure array. At the mid-point of the model, a harmonic source is placed to generate surface waves. A metastructure array with a total length $L = 160$ m (about 1340 resonator units) is placed on the right side, while surface waves on the left are used as a reference. Figure 5(a) shows the vertical displacement field map (red and blue color representing maximum and minimum displacement, respectively) for

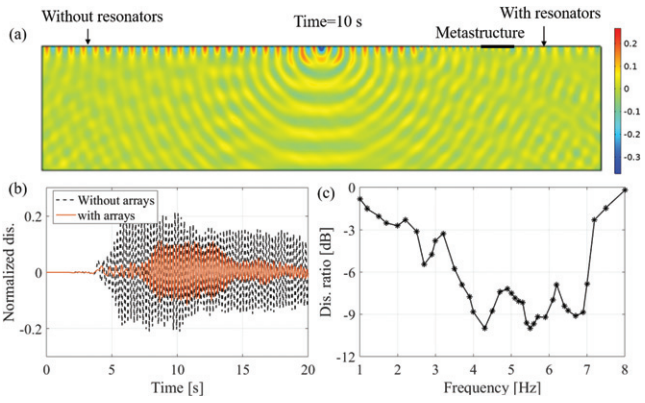

Fig. 5: (a) Harmonic response at 4.3 Hz with and without the resonators. (b) Time transient displacements in the z-direction of two positions (without and with resonators). (c) The displacement ratio of the model with resonators arrays to the model without arrays from 1 to 8 Hz.

soil without and with array at the time step $t = 10$ s for a 4.3 Hz prescribed displacement. The time transient displacements in the z-direction are recorded as shown in fig. 5(b) for models with and without the metastructure array.

To illustrate the phenomena more clearly, the displacement ratio is calculated from 1 to 8 Hz

$$d_{ratio} = 20 \log 10 \left(\frac{dis_{with}}{dis_{without}} \right). \tag{11}$$

As shown in fig. 5(c), the displacement reduction is over 6 dB from 3.5 to 7 Hz, which is satisfactory for protecting buildings against earthquakes at a wider frequency range.

In this letter, we proved the concept of simultaneously harvesting and mitigating seismic vibrations in a single device based on numerical simulation and preliminary experimental results. In the future, we hope to realize such a concept by lab and field experiments.

Conclusion. – This letter proposed an all-passive metastructure consisting of an array of nonlinear

electromagnetic resonators. The analytical model showed that the wave energy was stored and dissipated in the nonlinear resonators over a broaden frequency range due to the characteristics of nonlinearity and intrinsic frequency up-conversion. And through the electromagnetic coupling, the stored energy was able to convert into electricity passively. A two-unit array of such dual-functional resonators was experimentally tested to evaluate the energy harvesting performance. Results demonstrated a maximum RMS voltage output of 3 V subject to the base excitation of $0.5g$, an RMS power output of 3.7 mW and an energy harvesting efficiency of 22.26%. Through a rectifier bridge circuit, four R_TO's generated an DC voltage up to 15 V. Finally, the FEA simulation was conducted and exhibited that the earthquake mitigation over 6 dB was achieved from 3.5 to 7 Hz, which agrees well with the predication from the developed analytical model.

See the SM for the calculation of the magnetic force between two magnets and the LEDs power demonstration.

* * *

The authors wish to acknowledge financial support for this work from the Department of Energy ARPA-E (DE-AR0000531 and DE-AR0000945).

REFERENCES

[1] Shi Z. and Huang J., *Soil Dyn. Earthq. Eng.*, **50** (2013) 204.
[2] Cheng W., Wang J., Jonas U., Fytas G. and Stefanou N., *Nat. Mater.*, **5** (2006) 830.
[3] Brûlé S., Javelaud E. H., Enoch S. and Guenneau S., *Phys. Rev. Lett.*, **112** (2014) 133901.
[4] Marco M., Anastasiia K., Federico B. and Nicola M. P., *New J. Phys.*, **18** (2016) 083041.
[5] Colombi A., Roux P., Guenneau S., Gueguen P. and Craster R. V., *Sci. Rep.*, **6** (2016) 19238.
[6] Colombi A., Roux P. and Rupin M., *J. Acoust. Soc. Am.*, **136** (2014) EL192.
[7] Witarto W., Wang S. J., Yang C. Y., Nie X., Mo Y. L., Chang K. C., Tang Y. and Kassawara R., *AIP Adv.*, **8** (2018) 045307.
[8] Shi Z., Cheng Z. and Xiang H., *Soil Dyn. Earthq. Eng.*, **57** (2014) 143.
[9] Finocchio G., Casablanca O., Ricciardi G., Alibrandi U., Garescì F., Chiappini M. and Azzerboni B., *Appl. Phys. Lett.*, **104** (2014) 191903.
[10] Palermo A., Krödel S., Marzani A. and Daraio C., *Sci. Rep.*, **6** (2016) 39356.
[11] Palermo A., Vitali M. and Marzani A., *Soil Dyn. Earthq. Eng.*, **113** (2018) 265.
[12] Krödel S., Thomé N. and Daraio C., *Extreme Mech. Lett.*, **4** (2015) 111.
[13] Cottone F., Vocca H. and Gammaitoni L., *Phys. Rev. Lett.*, **108** (2009) 080601.
[14] Mann B. P. and Sims N. D., *J. Sound Vib.*, **319** (2009) 515.
[15] Jung S. M. and Yun K. S., *Appl. Phys. Lett.*, **96** (2010) 111906.
[16] Panigrahi S. R., Bernard B. P., Feeny B. F., Mann B. P. and Diaz A. R., *J. Sound Vib.*, **399** (2017) 216.
[17] Chen J., Wang Y. and Grisso B. L., *Sens. Actuators A Phys.*, **284** (2018) 66.
[18] Shen W., Zhu S., Zhu H. and Xu Y., *Smart Struct. Syst.*, **18** (2016) 449.
[19] Yang C. W., Lai Y. and Kim J., *Smart Mater. Struct.*, **26** (2017) 085005.
[20] Chen J. and Wang Y., *Appl. Phys. Lett.*, **114** (2019) 053902.
[21] Deng W. and Wang Y., *Appl. Phys. Lett.*, **109** (2016) 133903.
[22] Akoun G. and Yonnet J. P., *IEEE Trans. Magn.*, **20** (1984) 1962.
[23] Boechler N., Eliason J. K., Kumar A., Maznev A. A., Nelson K. A. and Fang N., *Phys. Rev. Lett.*, **111** (2013) 036103.
[24] Graff K. F., *Wave Motion in Elastic Solids* (Ohio State University Press, Columbus) 1975, p. 311.
[25] Sugino C., Leadenham S., Ruzzene M. and Erturk A., *J. Appl. Phys.*, **120** (2016) 134501.
[26] Mitcheson P. D., Yeatman E. M., Rao G. K., Holmes A. S. and Green T. C., *Proc. IEEE*, **96** (2008) 1457.